Available online at www.sciencedirect.com

ScienceDirect

journal homepage: http://www.elsevier.com/locate/rpor

Original research article

Simulation of positron emitters for monitoring of dose distribution in proton therapy

Mohsen Mashayekhi[a], *Ali Asghar Mowlavi*[a,b,*], *Sayyed Bijan Jia*[c]

[a] *Department of Physics, Hakim Sabzevari University, Sabzevar, Iran*
[b] *International Centre for Theoretical Physics (ICTP), Associate and Federation Schemes, Medical Physics Field, Trieste, Italy*
[c] *Department of Physics, University of Bojnord, Bojnord, Iran*

ARTICLE INFO

Article history:
Received 8 May 2016
Received in revised form
2 September 2016
Accepted 11 October 2016
Available online 31 October 2016

Keywords:
Proton therapy
β^+ activity distribution
Positron emitters
GEANT4 toolkit

ABSTRACT

Aim: The purpose of this work was to estimate the dependency between the produced positron emitters and the proton dose distribution as well as the dependency between points of annihilation and the proton dose distribution.

Background: One important feature of proton therapy is that, through the non-elastic nuclear interaction of protons with the target nuclei such as ^{12}C, ^{14}N and ^{16}O, it produces a small number of positron-emitting radioisotopes along the beam-path. These radioisotopes allow imaging the Bragg peak position which is related to the proton dose distribution by using positron emission tomography.

Methods: In this study, the GEANT4 toolkit was applied to simulate a soft and bone tissue phantom in proton therapy to evaluate the positron emitter productions and the actual annihilation points of β^+. Simulation was done by delivering pencil and spread-out Bragg peak (SOBP) proton beams.

Results: The findings showed that (^{15}O, ^{11}C, ^{13}N) and (^{11}C, ^{15}O, ^{38}K, ^{30}P, ^{39}Ca, ^{13}N) are the most suitable positron emitters in the soft and bone tissue respectively. By increasing the proton energy, the distance between the peak of annihilation profile and Bragg peak is almost constant, but the distance between the Bragg peak position and positron annihilation point peak in bone tissue is smaller than that in the soft tissue. The peak of β^+ activity distribution becomes sharper at higher proton energies.

Conclusions: There is a good relationship between the positions of positron annihilation profile and positron emitters radioactive decay. Also, GEANT4 is a powerful and suitable tool for simulation of nuclear interactions and positron emitters in tissues.

* *Corresponding author*. Fax: +98 51 44012520.
E-mail addresses: amolavi@ictp.it, amowlavi@hsu.ac.ir (A.A. Mowlavi).
http://dx.doi.org/10.1016/j.rpor.2016.10.004

1. Background

Nowadays, cancer is a major disaster around the world. Twenty-five percent of all deaths in Europe have been associated with different types of cancers. In fact, cancer is the main cause of mortality in the age range of 45–65 years.[1] The main goal in cancer treatment is to destroy the tumor tissues and spare the adjacent healthy tissues.[2]

Proton therapy is increasingly gaining acceptance in cancer treatment. The power of proton therapy is that the maximum radiation dose (at the Bragg peak) is deposited just before the end of the proton path. Beyond this point, the dose quickly falls down near zero. This characteristic enables proton beams to deliver a large radiation dose to the tumors while sparing critical distal organs. In order to achieve ideal proton treatment outcomes, an accurate calculation of tissue stopping power is needed to estimate range and proton beam dose. Despite these benefits, currently, there are many unanswered questions regarding proton therapy.[3] One of the most important unknowns is the uncertainty in the position of the Bragg peak. The exact determination of the peak position is difficult due to internal motions of the patient organs during the treatment course. Therefore, to adjust the Bragg peak position, it is essential to have an online monitoring system. Positron emission tomography (PET) is potentially a very useful and powerful tool for monitoring the dose distribution in proton therapy.[4–9] This method is based on the detection of 0.511 MeV photons, resulting from the annihilation of positrons emitted by positron emission radioactive decay. Positron emitters, such as ^{11}C, ^{13}N, ^{15}O are produced via non-elastic nuclear reaction of protons with the target nuclei of the irradiated tissue. After β^+ decay, positrons move through the matter and they continually lose their energy by coulomb scattering. Coincidence detection of the two collinear photons by PET camera makes it possible to determine the Bragg peak position in proton therapy.

Due to multiple scattering of the positron, its path in a tissue is far from a straight line, and its average penetration depth is shorter than its actual depth. This difference is described by a detour factor.[10,11] Since the positrons slow down by multiple scattering, e^+–e^- annihilation takes place practically at rest. Therefore, the angle between the momenta of the emitted photons is close to 180° and can be detected outside the patient body by a PET system. There are complexities in nuclear interactions and spatial relationship between delivered dose and β^+ activity. However, it needs some models to describe the complex physics of charged particle interactions. GEANT4 is a Monte Carlo code that is able to manage elementary particles and heavy ion interactions from the threshold up to cosmic range energies.

In this paper, we have done Monte Carlo simulations of biological tissues irradiated by pencil and spread-out Bragg peak (SOBP) proton beams to determine the main positron emitters (^{11}C, ^{13}N, ^{15}O, ^{38}K, ^{30}P, ^{39}Ca, ^{18}F) and the actual β^+ annihilation points for each type of tissue. These simulations have been done by GEANT4 Monte Carlo toolkit.

2. Materials and methods

Geant4, version 4.10.01, is a C++ toolkit for simulating the transport and interactions of particles in matter, modeling comprehensively physical processes over a wide range of energies.[12] First, protons are emitted from the point source without any dispersion in energy. For generating SOBP beams, discrete spectra with 68.2 and 119.15 MeV mean energies are simulated. Positron emitter productions and positron annihilation points are recorded as long as radioactive decay and pair annihilation process take place.

The models we used in the physics list contain the standard package and binary cascade model for EM and hadronic interactions. The geometry is a cubic phantom with dimensions of $60 \times 20 \times 20\ cm^3$. Here we have considered two different types of phantoms: soft tissue (0.1% H, 0.11% C, 0.02% N, 0.76% O) and bone tissue (0.063% H, 0.27% C, 0.027% N, 0.41% O, 0.002% Mg, 0.07% P, 0.002% S, 0.14% Ca) with density of 1 and 1/85 g/cm^3, respectively.[13]

3. Results and discussion

The simulations were performed using pencil and SOBP proton beams irradiating a soft and bone tissue by using the GEANT4 toolkit. The number of protons used in each set of the simulations was 4×10^6. Simulation results for yields of positron emitter nuclei per beam particles in beam direction for four different proton energies are listed in (Tables 1 and 2).

The results in Table 1, for the soft tissue, show that the yields of ^{15}O, ^{11}C, ^{13}N and ^{18}F are ordered and the yields are increased by the energy beam. However, in Table 2, ^{11}C has the highest yield instead of ^{15}O. Because the $^{12}C(p, pn)^{11}C$ and $^{16}O(p, pn)^{15}O$ cross sections are different in these types of tissues. The yields of other β^+-emitting nuclei, such as ^{18}F, are negligible.

The yields of positron emitter productions depend on the incident beam energy and composite material of the target and strongly depend on the modeling of nuclear interactions. So it takes some models to describe the complex physics of charge particle interactions. Also, the content of the considered isotopes in soft and bone tissues influences these yields.

With this analysis, it can be seen that ^{11}C and ^{15}O nuclei are the most suitable radioisotopes for monitoring the Bragg peak position in proton therapy. Most of the ^{11}C nuclei with 20.39 min half-life will survive for 10–20 min after stopping the proton irradiation.

The results regarding the distance of the Bragg peak and 50% peak fall-off in positrons annihilation points curve are listed in Table 3. Also in Table 3, the distances between the Bragg peak and peak of β^+-activity distributions are illustrated.

In order to use the PET method for dose monitoring, the employed calculation tool must well describe both the dose and β^+-activity distributions, like the GEANT4 toolkit. The production density results of ^{11}C, ^{13}N, ^{15}O, ^{38}K, ^{30}P, ^{39}Ca, ^{18}F and positrons annihilation points for bone and soft tissue phantom under proton pencil beam are presented in Figs. 1–4. The total dose deposited in the tissue is superimposed with a

Table 1 – Calculated yields of positron-emitting nuclei (per beam particle) produced by proton pencil beam in the soft tissue.

Positron emitter	50 MeV	100 MeV	150 MeV	200 MeV
^{15}O	0.0052 ± 0.0003	0.0147 ± 0.0006	0.0260 ± 0.0007	0.0390 ± 0.0009
^{11}C	0.0024 ± 0.0002	0.0089 ± 0.0004	0.0158 ± 0.0006	0.0234 ± 0.0007
^{13}N	0.0002 ± 0.0007	0.0016 ± 0.0001	0.0035 ± 0.0002	0.0057 ± 0.0003
^{18}F	0.0000 ± 0.0000	0.0000 ± 0.0004	0.0000 ± 0.0009	0.0000 ± 0.0001

Table 2 – Calculated yields of positron-emitting nuclei (per beam particle) produced by proton pencil beam in bone tissue.

Positron emitter	50 MeV	100 MeV	150 MeV	200 MeV
^{11}C	0.0041 ± 0.0003	0.0117 ± 0.0005	0.0201 ± 0.0007	0.0293 ± 0.0008
^{15}O	0.0029 ± 0.0002	0.0083 ± 0.0004	0.0149 ± 0.0006	0.0227 ± 0.0007
^{38}K	0.0004 ± 0.0001	0.0019 ± 0.0002	0.0033 ± 0.0002	0.0050 ± 0.0003
^{30}P	0.0005 ± 0.0001	0.0014 ± 0.0001	0.0026 ± 0.0002	0.0041 ± 0.0003
^{39}Ca	0.0004 ± 0.0001	0.0012 ± 0.0001	0.0022 ± 0.0002	0.0034 ± 0.0002
^{13}N	0.0002 ± 0.0007	0.0010 ± 0.0001	0.0024 ± 0.0002	0.0037 ± 0.0003
^{18}F	0.0000 ± 0.0004	0.000 ± 0.001	0.000 ± 0.003	0.0001 ± 0.0005

Table 3 – Distance of 50% peak falloff in annihilation profile and Bragg peak and distance between peak of annihilation profile and Bragg peak by proton pencil beams in soft and bone tissues.

Energy (MeV)	Bone tissue		Soft tissue	
	50% β^+ peak falloff-Bragg peak (cm)	β^+ peak-Bragg peak (cm)	50% β^+ peak falloff-Bragg peak (cm)	β^+ peak-Bragg peak (cm)
50	0.271 ± 0.001	0.48 ± 0.01	0.509 ± 0.001	1.20 ± 0.02
100	0.188 ± 0.001	0.48 ± 0.01	0.506 ± 0.001	1.08 ± 0.02
150	0.173 ± 0.001	0.48 ± 0.01	0.440 ± 0.001	1.20 ± 0.02
200	0.105 ± 0.008	0.60 ± 0.01	0.321 ± 0.001	1.20 ± 0.02

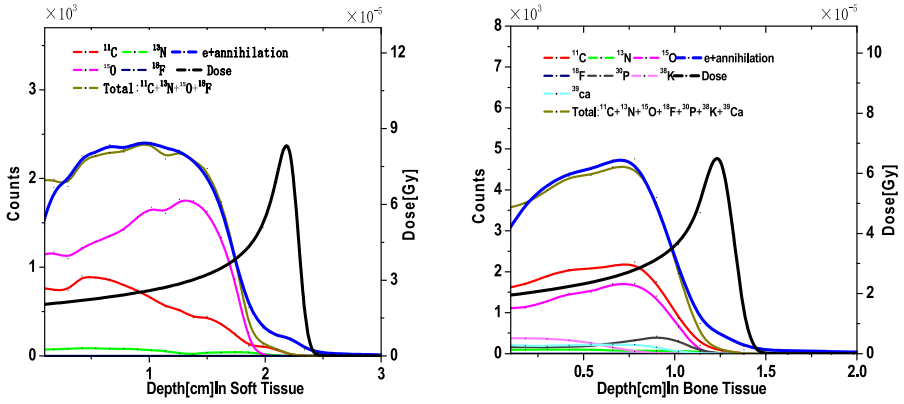

Fig. 1 – Calculated depth dose profiles and positron emitter productions, their sum and actual e^+annihilation points for 50 MeV proton pencil beam in soft and bone tissue phantom.

right-side vertical scale in the same Figs. for in depth comparison. The obtained results show that the distance between the peak of the annihilation profile and the Bragg peak is almost constant for different initial energies. The distance between the annihilation depth profile and Bragg peak is mainly determined by the rest range of the protons when falling below the nuclear reaction energy threshold. So, we expect this difference to be almost constant for different initial proton energies. But the 50% peak fall-off in annihilation profile is closer to the Bragg peak at higher proton energies.

The distance between the Bragg peak position and positron annihilation point peak in bone tissue is smaller than the soft tissue. It may come from the different interaction cross sections and enhanced relative electronic stopping-power in bone compared to soft tissue. Electromagnetic and nuclear interactions are responsible for the dose deposition and positron emitter productions, respectively. With the increase of electron density and electronic stopping power, the depth of proton beams in bone tissue is shorter than soft tissue. In addition, nuclear interactions are different in these types of tissues.

It can be seen that in the soft tissue the total positron emitters distribution of ^{11}C, ^{13}N, ^{15}O and ^{18}F is close to β^+-activity distributions by all positron emitters. Therefore, these four nuclei are important and sufficient in our calculation. But in the bone tissue positron emitter distributions do not match

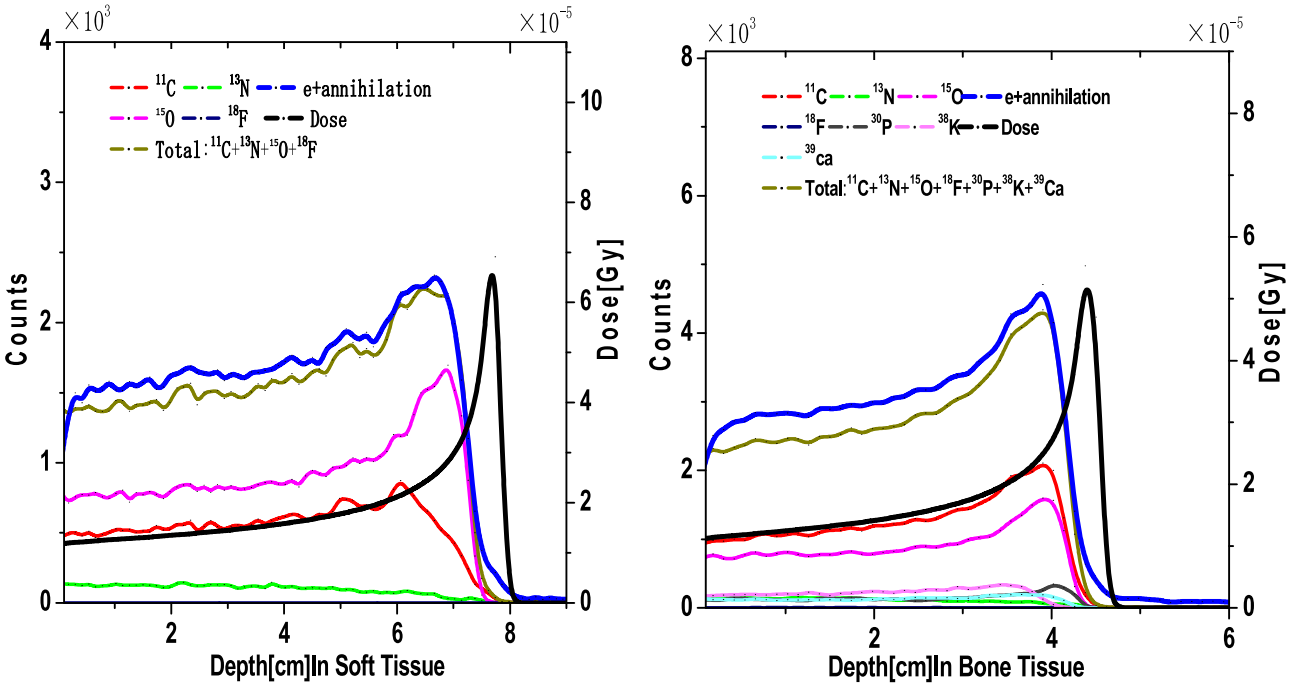

Fig. 2 – Calculated depth dose profiles and positron emitter productions, their sum and actual e^+-annihilation points for 100 MeV proton pencil beam in soft and bone tissue phantom.

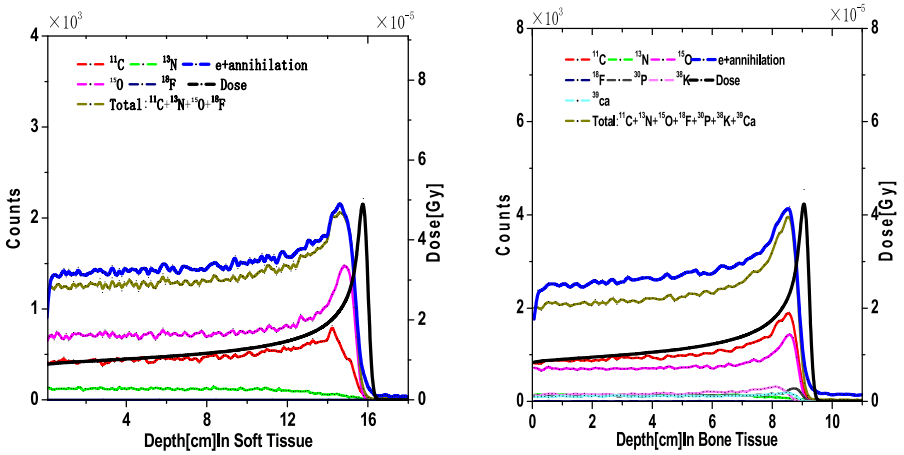

Fig. 3 – Calculated depth dose profiles and positron emitter productions, their sum and actual e^+-annihilation points for 150 MeV proton pencil beam in soft and bone tissue phantom.

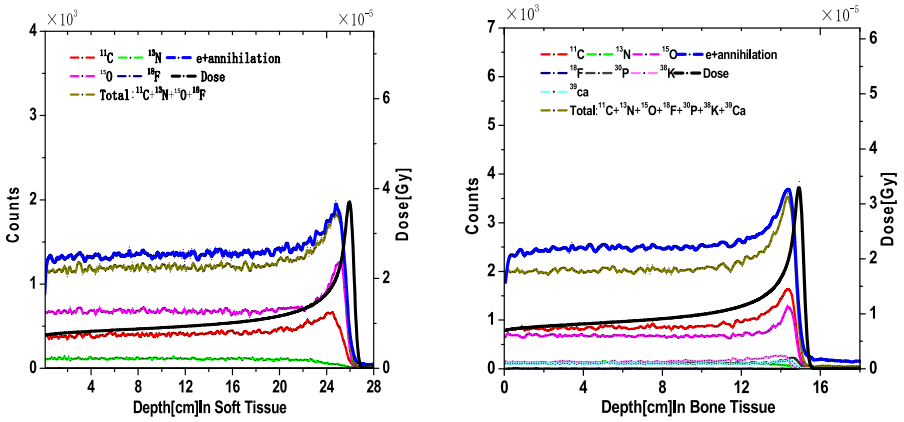

Fig. 4 – Calculated depth dose profiles and positron emitter productions, their sum and actual e^+-annihilation points for 200 MeV proton pencil beam in soft and bone tissue phantom.

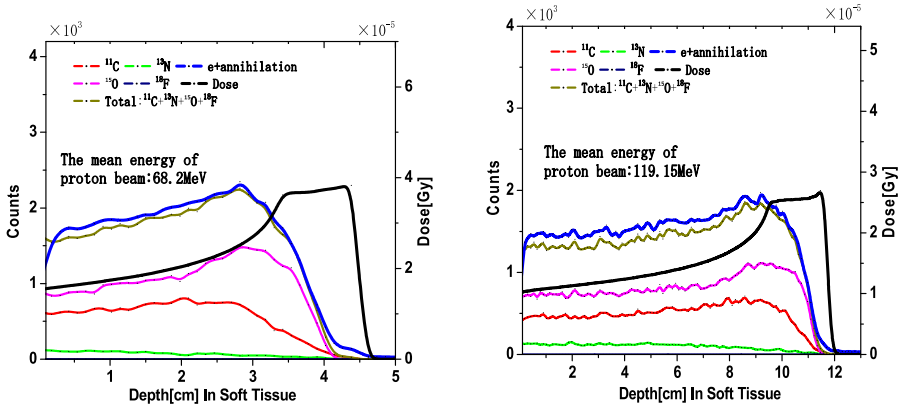

Fig. 5 – Calculated depth dose profiles and positron emitter productions, their sum and actual e^+-annihilation points for SOBP proton beams in soft tissue phantom.

well with the β^+-activity distributions; it means that some other positron emitters (^{38}K, ^{30}P, ^{39}Ca) must be considered.[14,15]

Fig. 5 shows positron emitter productions and annihilation points for SOBP proton beams in the soft tissue. In this case, there are wide peaks in β^+-activity and positron emitter distribution since there is a spectrum in protons beam energy. When the proton energy falls down below the neutron emission threshold, the production of β^+-activity will be stopped, so no β^+-emitters are produced by protons before the Bragg peak in these energies. It is necessary to mention that some of ^{11}C and ^{15}O nuclei are produced in the target by secondary particles like p, n and β^+-particles in the projectile fragmentation. The contribution of such processes is small, but still visible beyond the Bragg peak.[16] By increasing the proton energy, the peak of β^+ activity distribution becomes sharper as shown in Figs. 1–4.

4. Conclusion

In this simulation, the results have been calculated during proton irradiation by pencil and SOBP beams in soft and bone tissue. Our results show that there is a strong correlation between the position of positron annihilation profile and positron emitters radioactive decay. By increasing the proton energy, the distance between the peak of annihilation profile and the Bragg peak is almost constant. But the 50% peak fall-off in annihilation profile is closer to the Bragg peak at higher proton energies. This is important for online PET system based on the verification of dose distributions delivered by charged particles. In the soft tissue ^{15}O, ^{11}C, ^{13}N and in the bone tissue ^{11}C, ^{15}O, ^{38}K, ^{30}P, ^{39}Ca, ^{13}N are the main positron emitters produced by proton beam, respectively.

Conflict of interest

None declared.

Financial disclosure

None declared.

Acknowledgements

Authors would like to thanks Hakim Sabzevari University for the supports.

REFERENCES

1. Niederlaender E. Causes of death in the EU. *Stat focus* 2006;**10**:2–11.
2. Yock TI, Tarbell NJ. Technology insight: proton beam radiotherapy for treatment in pediatric brain tumors. *Nat Clin Pract Oncol* 2004;**1**:97–103.
3. Lin L, Vargas C, Hsi W, et al. Dosimetric uncertainty in cancer proton radiotherapy. *Med Phys* 2008;**35**:4800–7.
4. Enghardt W, Debus J, Haberer T, et al. Positron emission tomography for quality assurance of cancer therapy with light ion beams. *Nucl Phys A* 1999;**654**:1047–50.
5. Parodi K, Enghardt W. Potential application of PET in quality assurance of proton therapy. *Phys Med Biol* 2000;**45**:N151–6.
6. Parodi K, Paganetti H, Shih HA, et al. Patient study of in vivo verification of beam delivery and range, using positron emission tomography and computed tomography imaging after proton therapy. *Int J Radiat Oncol* 2007;**68**:920–34.
7. Oelfke U, Lam GKY, Atkins MS. Proton dose monitoring with PET: quantitative studies in Lucite. *Phys Med Biol* 1996;**41**:177–96.
8. Parodi K, Enghardt W, Haberer T. In-beam PET measurements of β^+ radioactivity induced by proton beams. *Phys Med Biol* 2001;**47**:21–36.
9. Min CH, Zhu X, Winey BA, et al. Clinical application of in-room positron emission tomography for in vivo treatment monitoring in proton radiation therapy. *Int J Radiat Oncol* 2013;**86**:183–9.
10. Fernández-Varea JM, Andreo P, Tabata T. Detour factors in water and plastic phantoms and their use for range and depth scaling in electron-beam dosimetry. *Phys Med Biol* 1996;**41**:1119–39.
11. Peng H, Levin CS. Study of PET intrinsic spatial resolution and contrast recovery improvement for PET/MRI systems. *Phys Med Biol* 2012;**57**:N101–15.
12. Agostinelli S, Allison J, Amako K, Apostolakis J, Araujo H, Arce P. Geant4—a simulation toolkit. *Nucl Instrum Methods A* 2003;**506**:250–303.
13. http://geant4.web.cern.ch/geant4/G4UsersDocuments.

14. Aya M, Teiji N, Takashi O, et al. Measurement and verification of positron emitter nuclei generated at each treatment site by target nuclear fragment reactions in proton therapy. *Med Phys* 2010;**37**:4445–55.
15. Katia P, Thomas B, Thomas H. Comparison between in-beam and offline positron emission tomography imaging of proton and carbon ion therapeutic irradiation at synchrotron-and cyclotron-based facilities. *Int J Radiat Oncol* 2008;**71**:945–56.
16. Anna D, Monika Paluch F, Adam K. The determination of a dose deposited in reference medium due to (p, n) reaction occurring during proton therapy. *Rep Pract Oncol Radiother* 2014;**19**:S3–8.